Ultrasound in Med. & Biol., Vol. 32, No. 11, pp. 1639–1648, 2006

0301-5629/06/$–see front matter

ELSEVIER

doi:10.1016/j.ultrasmedbio.2006.05.006

● *Original Contribution*

EXAMINATION OF CANCER IN MOUSE MODELS USING HIGH-FREQUENCY QUANTITATIVE ULTRASOUND

MICHAEL L. OELZE,*‡ and JAMES F. ZACHARY†‡

*Bioacoustics Research Laboratory, Department of Electrical and Computer Engineering; †Department of Pathobiology; and ‡Department of Bioengineering, University of Illinois, Urbana, IL, USA

(*Received* 21 *November* 2005; *revised* 27 *April* 2006; *in final form* 4 *May* 2006)

Abstract—Two mouse models of mammary cancer (a carcinoma and sarcoma) were examined using quantitative ultrasound (QUS). Scatterer property estimates, *i.e.*, the average scatterer diameter (ASD) and average acoustic concentration (AAC), were estimated from regions-of-interest (ROIs) inside the tumors. Initially, the spherical Gaussian model was used over an analysis bandwidth of 10 to 25 MHz to obtain ASD and AAC estimates. ASD estimates were 31.7 ± 9.36 μm and 31.0 ± 7.20 μm for the carcinomas and sarcomas, respectively. AAC estimates were 6.77 ± 8.75 dB[mm^{-3}] and 9.87 ± 9.24 dB[mm^{-3}], respectively. The initial ASD and AAC estimates did not yield statistically significant differences between the two kinds of tumors ($p = 0.83, 0.86$ for the ASD and AAC estimates, respectively). However, optical photomicrographs revealed distinct morphologic differences between the tumors. F-tests on the average power spectra from the tumors revealed statistically significant differences between the spectra over the range of 16 to 25 MHz. ASD and AAC estimates using the spherical Gaussian model were then obtained over the new analysis bandwidth of 16 to 25 MHz. The new ASD estimates were 42.1 ± 4.01 μm and 32.1 ± 3.81 μm for the carcinomas and sarcomas, respectively. The new AAC estimates were 16.4 ± 17.1 dB[mm^{-3}] and 36.4 ± 11.9 dB[mm^{-3}], respectively. Statistically significant differences were observed for both the ASD and AAC estimates when using the new analysis bandwidth. Structural differences between the tumors were revealed by both QUS and optical photomicrographs. (E-mail: oelze@uiuc.edu) © 2006 World Federation for Ultrasound in Medicine & Biology.

Key Words: **Quantitative ultrasound, Backscatter, Cancer detection, Tissue characterization, Breast cancer, Parametric imaging.**

INTRODUCTION

Qualitative ultrasound (QUS) has been used successfully to diagnose and monitor disease, such as cancer. Furthermore, QUS approaches have been used to differentiate different kinds of tissues (Insana et al. 1991; Lizzi et al. 1983, 1987; Miller et al. 1983; Oelze et al. 2002). QUS images, images enhanced by scatterer parameters like the average scatterer diameter (ASD) and average acoustic concentration (AAC), have been constructed for test phantoms (Insana and Hall 1990) and tissues (Feleppa et al. 1986, 1988, 1999; Insana and Brown 1993; Lizzi et al. 1997a; Silverman et al. 1995). The AAC is defined as the number of scatterers per unit volume multiplied by the squared difference in acoustic impedance between the scatterers and surrounding medium (Feleppa et al. 1988). In clinical settings, QUS has been used to successfully diagnose prostate cancer, ocular tumors and cardiac abnormalities (Feleppa et al. 1997; Lizzi et al. 1997a; Miller et al. 1983). QUS backscattering techniques have also been used to characterize different aspects of tissue microstructures (Lizzi et al. 1997b). Noteworthy are the pioneering works of Lizzi et al. (1983, 1987) that demonstrated theoretically and experimentally the ability to ultrasonically quantify ocular, liver and prostate tissues.

Feleppa et al. (1986) found that the effective scatterer size (ASD) in ocular tumors was a strong indicator of malignant cancer. Larger ASDs were observed in malignant tumors as opposed to surrounding normal tissues. The AAC was less sensitive for cancer detection than the scatterer size but was helpful for diagnostically distinguishing between ambiguous cases (Lizzi et al. 1987). Feleppa et al. (1996) and Balaji et al. (2002) also demonstrated that QUS provided greater diagnostic accuracy in prostate-cancer detection and lesion localization than all other noninvasive techniques combined. Although initial studies by Feleppa et al. (1986) sug-

Address correspondence to: Michael L. Oelze, Beckman Institute, 405 N Mathews, University of Illinois at Urbana-Champaign, Urbana, IL 61801, USA. E-mail: oelze@uiuc.edu

gested that the AAC was less sensitive for detecting ocular tumors than the scatterer size (Silverman et al. 1997), later studies (Feleppa et al. 1997) suggested that there were large differences in both ASD and AAC between malignant and nonmalignant regions, emphasizing a potentially important role for the latter.

Anisotropy measurements of scattering in the kidney revealed that changes in the effective scattering strength (same as the AAC defined in this study) were responsible for the anisotropy of backscatter and not changes in scatterer size (Insana et al. 1991). In that work, the glomeruli ($\approx$200 μm) and afferent and efferent arterioles ($\approx$50 μm) were identified as the principal structures responsible for scattering at diagnostic ultrasound frequencies (1 to 15 MHz). These studies led to investigations into using QUS images of the scatterer properties to detect changes in renal microanatomy (Garra et al. 1994; Hall et al. 1996; Insana et al. 1992, 1995). QUS imaging techniques were capable of differentiating among conditions that caused increased cortical echogenicity and structural changes like glomerular hypertrophy. Furthermore, ASD estimates agreed well with measurements of those structures made using biopsy samples.

In a previous study, Oelze et al. (2004) were able to distinguish between benign fibroadenomas and mammary carcinomas in rodent models of breast cancer using QUS techniques. Furthermore, the estimated scatterer properties were related to actual tissue morphology by comparisons with optical photomicrographs of stained tissue sections. Success in using ultrasound to diagnose breast cancer in humans has been limited. System-dependent techniques for evaluating echogenic features of B-mode images have had limited success in detecting and classifying breast cancer. Several studies in the literature describe improved means of diagnosing breast abnormalities, specifically distinguishing cystic from solid tumors and differentiating among solid breast tumors, in an effort to improve diagnostic accuracy. One well-known study is by Stavros et al. (1995), who described a set of criteria, *e.g.*, relative "echogenicity," shadowing, speculation, lobulation features, *etc.*, for diagnosing breast lesions. This work was followed by an effort to encode many of the criteria into an automated algorithm (Drukker et al. 2002). The limited success of system-dependent techniques for detecting and classifying breast cancer could be improved by augmentation with QUS analysis.

The successes of QUS in earlier studies of ocular tumors, renal tissues, prostate cancer, and breast lesions suggested that variance in scatterer property estimates from tissues was manageable and did not destroy the effectiveness of the techniques. On the basis of those previous successes, two malignant cases of mammary cancer in mouse models were studied using QUS techniques: a carcinoma and a sarcoma.

MATERIALS AND METHODS

Animal use

The experimental protocol was approved by the Institutional Animal Care and Use Committee of the University of Illinois and satisfied all campus and National Institutes of Health rules for the humane use of laboratory animals.

Mouse carcinomas

A mouse mammary tumor cell line (4T1 [CRL-2539]) was purchased from American Type Culture Collection (ATCC, Manassas, VA, USA). This cell line was chosen because of its homogeneous cytologic characteristics and because the tumors are models for stage IV human breast cancer in growth patterns (Aslakson and Miller 1992; Pulaski and Ostrand-Rosenberg 1998; Pulaski et al. 2000). For example, the 4T1 mouse mammary tumor spontaneously metastasizes while the primary tumor is in place, analogous to human tumors (Pulaski et al. 1998) Further, the locations of these metastases are common between the mouse and human malignancies.

The 4T1 cells have relatively uniform morphology: they are oval to polygonal in shape with large prominent nuclei. Extracellular matrix was minimal to nonapparent. We used these cells as an *in vivo* model for uniform scattering statistics in tissues. In the context of QUS imaging, the tumors from this cell line mimic the appearance of ductal carcinoma *in situ* (DCIS) in humans. Cells related to DCIS in humans appear to be monomorphic in nature (unless surrounded by Paget cells that are pleomorphic with abundant cytoplasm) and can consist of sheets of carcinoma cells (Cotran et al. 1999). Similarly, the 4T1 mouse mammary tumors contain sheets of carcinoma cells that appear to be monomorphic in nature.

The 4T1 cells were stored at –70°C, thawed at 37°C in a water bath, grown in Roswell Park Memorial Institute (RPMI) 1640 medium with 10% fetal bovine serum (FBS) and antibiotic/antifungal supplements (ATCC), and incubated at 37°C at 100% humidity and 5% CO_2. Cells were grown in 75-cm^2 tissue culture flasks (T-75, Corning Incorporated, Corning, NY, USA). When cells were 80% confluent (*i.e.*, adherent cell line), they were rinsed with RPMI 1640 medium lacking FBS or supplements and then covered with 2.0 mL of Trypsin-EDTA (ATCC) to detach the cells from the flask. The cells were gently and repetitively drawn through a 10-mL pipette to individualize the cells. The number of cells present in an 80% confluent flask was determined to be approximately 10^7 cells/mL. The approximate number was calculated by counting the number of cells in a small area of the

flask and extrapolating to estimate the total number of cells contained in the entire flask.

Detached cells were washed two times with 10 mL of RPMI 1640 medium lacking FBS or supplements and resuspended in RPMI 1640 medium lacking FBS or supplements to concentration of 10^5 cells/mL. The abdominal mammary fat pad of anesthetized 8- to 16-week-old female BALB/c mice (Harlan, Indianapolis, IN, USA) was injected with 0.1 mL of suspended 4T1 cells (approximately 10^4 cells). The injected cells initiated visible tumor growth in 100% of mice within 8 to 10 days postinjection (Pulaski and Ostrand-Rosenberg 1998). Tumors in the mice were allowed to grow until they had reached 1 cm in diameter (typically three to four weeks post injection). Mice were then anesthetized and humanely killed under anesthesia by cervical dislocation. The tumors were ultrasonically imaged *in situ* by recording the backscattered RF signals (see Ultrasound scanning procedures). The scanning system consisted of mechanically translating a single-element transducer across the tumor. The animals were euthanized before scanning because tumor motion due to breathing in live animals during scans caused distortion in the subsequent ultrasound images (humans can compliantly hold their breath for several seconds). The trade-off for scanning euthanized animals is that the effects of blood flow on ultrasound backscatter could not be characterized.

Ten 4T1 tumor-bearing mice were analyzed using QUS. For each mouse, the tumor and surrounding area were shaved with electric clippers and depilated (Nair®). Each euthanized mouse was placed in a holder in a tank of degassed water at 37°C for scanning with an ultrasonic transducer. After scanning, tumors were excised, fixed in 10% neutral-buffered formalin, processed and embedded in paraffin, sectioned at 5 μm, and stained with hematoxylin and eosin (H&E) for routine histologic evaluation by light microscopy. The tumors were diagnosed as mouse mammary carcinomas following histopathologic evaluation.

Mouse sarcomas

A mouse sarcoma tumor cell line (Englebreth-Holm-Swarm, EHS [CRL-2539]) was purchased from American Type Culture Collection (Manassas, VA, USA). This cell line was chosen because it produced abundant extracellular materials and basement-membrane components (laminin, collagen IV, entactin, and heparan sulfate proteoglycan) (Kleinman et al. 1986; Timpl et al. 1979). Like the carcinoma cell line, the cells were relatively uniform in morphology: they were oval to polygonal in shape with large prominent nuclei and arranged in groups usually containing less than 20 cells per group. Groups of cells were distributed at random in the abundant extracellular matrix, thus, in many areas such groups of cells were widely separated, which resulted in identifiable structural differences when compared with the carcinomas. We used these cells as an *in vivo* model for uniform scattering statistics in tissues and to examine the role of extracellular matrix in ultrasonic scattering.

Mice were weighed and then anesthetized with ketamine hydrochloride (87.0 mg/kg) and xylazine (13.0 mg/kg) administered intraperitoneally before injection with EHS cells. Initially the EHS cells were stored at –70°C. Culturing procedures consisted of thawing the cells at 37°C in a water bath and injecting them into three C57BL/6 mice. The cells were cultured *in vivo*. The mice would develop visible tumors after 14 to 21 days post inoculation. When the tumors were about 1 cm in diameter, the tumors were harvested from the mice, minced and injected intramuscularly (over the hind limb) into C57BL/6 mice. The number of mice injected depended on the tumor yield from the three mice. Some of the newly injected mice were then used to continue the culturing process and some were used in the QUS analysis.

The mice to be analyzed with QUS were examined daily for tumor progression. When tumors reached a diameter of 1.0 cm (usually about 14 to 21 days after inoculation), mice were anesthetized and humanely euthanized under anesthesia by cervical dislocation. The tumors of the mice were scanned *in situ* ultrasonically and analyzed using QUS.

Ten EHS tumor-bearing mice were used in the study. For each mouse, the tumor and surrounding area were immediately shaved with electric clippers and depilated (Nair®). The mouse was then placed on a holder in a tank of degassed water at 37°C for scanning with an ultrasonic transducer. After scanning, the EHS-cell tumors were excised, processed, and evaluated as previously described for 4T1-cell tumors.

Ultrasound scanning procedures

A single-element, weakly focused transducer was used to scan the mice. The transducer had a measured center frequency of 20 MHz at the focus and a 75% –6-dB pulse/echo bandwidth that extended from 10 to 25 MHz. The aperture diameter of the 20-MHz transducer was 6 mm with a focus measured at 22 mm.

This transducer was interfaced with a Panametrics 5900 pulser/receiver. The received radiofrequency (RF) signals were acquired using a digital oscilloscope (Lecroy 9354TM, Chestnut Ridge, NY, USA) and downloaded to a PC computer for postprocessing. The oscilloscope digitized using 8-bit samples at a sampling rate of 200 MS/s. The transducers were moved laterally across the tumor by a micropositioning system with a distance of 50 μm between adjacent scan lines. The

attenuation for both kinds of tumors was 0.4 dB MHz^{-1} cm^{-1} based on insertion loss measurements made using sliced carcinoma and sarcoma tumor tissues.

Estimation routines

Acoustic-scattering theories for biologic tissues assume that the tissues can be modeled as inhomogeneous fluids (Insana and Brown 1993). Scattering occurs when an acoustic wave interacts with a region that has different acoustic impedance relative to the surrounding tissue or fluid. Acoustic signals backscattered from biologic tissues contain information about the size, shape, number and relative acoustic impedance of the scattering regions within the tissues. Analysis of the frequency content of backscattered signals (the normalized backscattered power spectrum) from tissues allows the estimation of certain average scatterer properties. These estimates represent ensemble averages of scatterer properties from specified ROIs.

Estimates of the average scatterer properties are found by comparing the normalized backscattered power spectrum of the RF signal gated from each ROI to a theoretical backscattered power spectrum. The backscattered power spectrum is the squared magnitude of the Fourier transform of the range gated RF signal. The theoretical backscattered power spectrum has been modeled from a three-dimensional (3-D) spatial autocorrelation function (SAF) describing the shape and distribution of scatterers in the medium (Insana et al. 1991; Insana and Brown 1993; Lizzi et al. 1987, 1997a; Oelze et al. 2002). The SAF models assume plane wave incidence, the Born approximation (Ishimaru 1978), single scattering, and the absence of shear waves (Insana et al. 1990; Morse and Ingard 1968).

An SAF model that has been used commonly to describe soft tissue scattering is the spherical Gaussian model. The spherical Gaussian model has been used for many years and for many applications to obtain estimates of scatter properties (Lizzi et al. 1997a; Nassiri and Hill 1986; Nicholas 1982). The spherical Gaussian model has been used because at low frequency the shape of the normalized backscattered power spectrum appeared to fit many tissue scattering measurements. Furthermore, the properties of the spherical Gaussian model allowed rapid classification schemes because it could be linearized in log space (Oelze et al. 2002).

A theoretical power spectrum has been constructed that incorporated range gating effects using a Hanning window and lateral beam pattern effects by Lizzi et al. for the spherical Gaussian scatterers (Lizzi et al. 1983, 1987, 1997a; Feleppa et al. 1986),

$$W_{theor}(f) = \frac{185 L q^2 a_{eff}^6 n_z f^4}{\left[1 + 2.66 f (q a_{eff})^2\right]} e^{-12.3 f^2 a_{eff}^2}, \qquad (1)$$

where f is the frequency (MHz), a_{eff}, is the effective scatterer radius (mm), n_z, the AAC of scatterers (mm^{-3}), L is the axial length of the range gated region (Hanning window) and q is the ratio of the aperture radius to distance from the ROI. The effective scatterer radius represents the correlation length associated with a spatial impedance profile described by a Gaussian function. The ASD was estimated by doubling the effective scatterer radius. Equation (1) describes the scattering from an ROI located spatially within the depth of field of a weakly focused transducer where the wavefront can be assumed to be planar. The AAC is defined as the number density of scatterers times the square of the impedance mismatch, *i.e.*, $\frac{Z_{scat} - Z_{back}}{Z_{back}}$, between scatterer and background.

The measured backscattered power spectrum for an ROI was constructed by averaging the backscattered power spectra measured from the echo signals of the set of scan lines within the ROI. The measured backscattered power spectrum is given by (Insana and Hall 1990),

$$W_{comp}(f) = \frac{1}{N} A(f, L) \sum_{n=1}^{N} \frac{\left| FT\{p_n(t)\} \right|^2}{W_{ref}(f)}, \qquad (2)$$

where $FT\{p_n(t)\}$ represents the Fourier transform of the gated RF signal of the nth scan line, N is the number of gated scan lines contained within an ROI, $A(f,L)$ is a frequency-dependent attenuation-compensation function (Oelze and O'Brien 2002) and $W_{ref}(f)$ is a reference power spectrum. The reference power spectrum was obtained by recording RF signals from reflections off a smooth planar surface of known reflectivity normal to the transducer beam axis. The planar reflector was translated from location at the front of the depth of field of the transducer to the back of the depth of field with a distance of 75 μm (the wavelength at 20 MHz) between steps. At each point the RF signal reflected from the smooth planar surface was recorded. The reference power spectrum for an ROI was calculated by averaging the squared magnitude of the Fourier transform of each reflected RF signal corresponding to the axial location of the ROI. The effects of the equipment on the power spectrum measurement were factored out by dividing by the reference power spectrum (Insana and Hall 1990; Lizzi et al. 1983; Oelze et al. 2002). Dividing by the reference power spectrum normalized the measured backscattered power spectrum. The measured backscattered power spectrum was compensated for attenuation losses according to the frequency-dependent attenuation-

compensation function, $A(f,L)$, derived for echo signals gated with Hanning windows (Oelze and O'Brien 2002).

Estimates of the scatterer properties were made using the technique of Oelze et al. (2002) by comparing the logarithm of the measured backscattered power spectrum, eqn (2), with the logarithm of the theoretical power spectrum, eqn (1) (Oelze et al. 2002),

$$10\log_{10}W_{comp}(f) \approx 10\log_{10}f^4 + m(a_{eff},\ q)f^2 + b(n_z,\ a_{eff},\ L,\ q). \quad (3)$$

Subtracting $10\log_{10}f^4$ from both sides of eqn (3) and letting $x = f^2$ yields

$$y = 10\log_{10}W_{comp}(\sqrt{x}) - 10\log_{10}x^2 \approx m(a_{eff},\ q)x + b(n_z,\ a_{eff},\ q,\ L). \quad (4)$$

Equation (4) describes a straight line *vs.* x where the slope, m, is a function of a_{eff} and q, and the intercept, b, is a function of a_{eff}, n_z, q, and L. The quantity q is determined by the characteristics of the operating transducer and L is known. To obtain the scatterer estimates, least-squares analysis was used to find the best-fit slope and intercept from the log of the averaged backscattered power spectrum of eqn (4) (Oelze et al. 2002). Once the average effective scatterer radius (ASD) was estimated from the slope of eqn (4), the AAC was estimated from the intercept and estimate of the ASD. Typically, AAC values span a large dynamic range. Therefore, estimates of AAC were expressed in a decibel scale,

$$n_{z_{dB}} = 10\log n_z, \quad (5)$$

referenced to an acoustic concentration, n_z, equal to unity.

Construction of quantitative ultrasound images

Before QUS images were constructed, B-mode images were generated from the RF data acquired in the mouse scans. From the B-mode images, ROIs were selected inside the tumors where the B-mode images appeared to be homogeneous (no interfaces or large echoes). The axial length of an ROI corresponded to the range-gated RF echo with length of 1.5 mm. The lateral length of an ROI was also held at 1.5 mm (corresponding to 30 scan lines separated by 50 μm). Estimates of scatterer properties were made for each ROI from the RF signals using QUS analysis and eqn (4). ROIs were chosen within the tumor so that axially and laterally an overlap of 66% existed from one ROI to the next.

Images revealing the spatial mapping of the scatterer-property estimates within the tumor were created by depicting the scatterer-property estimate at a particular location with a specific pixel color. Each pixel represented the average scatterer-property estimates from three or more overlapping ROIs. The colored pixels were then superimposed on the original grey-scale B-mode image of the tumor to form the enhanced QUS image.

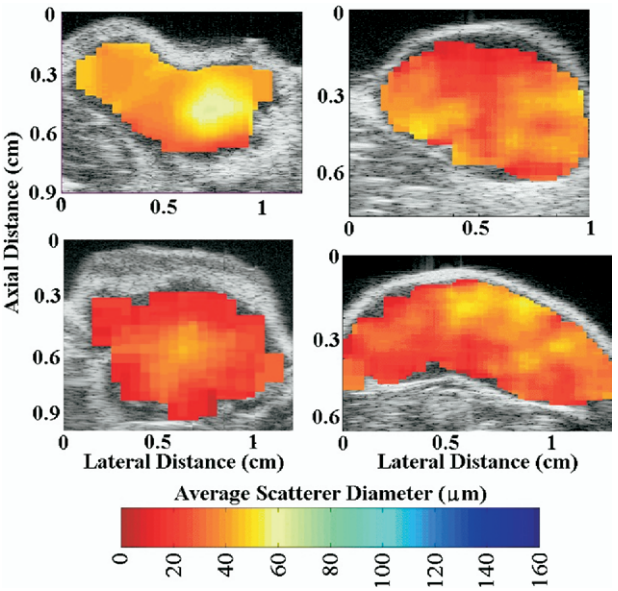

Fig. 1. Representative ASD images of mouse carcinomas (left panel) and mouse sarcomas (right panel).

RESULTS

Enhanced QUS images of the carcinomas and sarcomas utilizing the estimates of the ASDs are displayed in Fig. 1. Initial estimates were obtained using the spherical Gaussian model with an analysis bandwidth of 10 to 25 MHz. The colorbar in Fig. 1 corresponds to scatterer diameter estimates ranging from 0.0 to 160.0 μm. The large range of ASD values was used because previous QUS studies of benign mammary fibroadenomas in rodent models revealed estimated ASDs of as much as 160.0 μm (Oelze et al. 2004) Examination of the QUS images does not allow distinguishing of carcinomas from the sarcomas. The ASD estimates for both tumors are given in the histogram of Fig. 2a. The average estimated ASDs for both tumors were 31.7 $\pm$ 9.36 μm and 31.0 $\pm$ 7.20 μm for the carcinomas and sarcomas, respectively. Analysis of variance (ANOVA) was used to determine statistically significant differences between the ASD estimates from the carcinomas and sarcomas. A statistically significant difference was not observed between the carcinomas and sarcomas from the ASD estimates (p = 0.83).

Enhanced QUS images of the carcinomas and sarcomas utilizing the estimates of the AAC are displayed in Fig. 3. The large range of AAC denoted by the colorbar was chosen based on previous QUS studies of

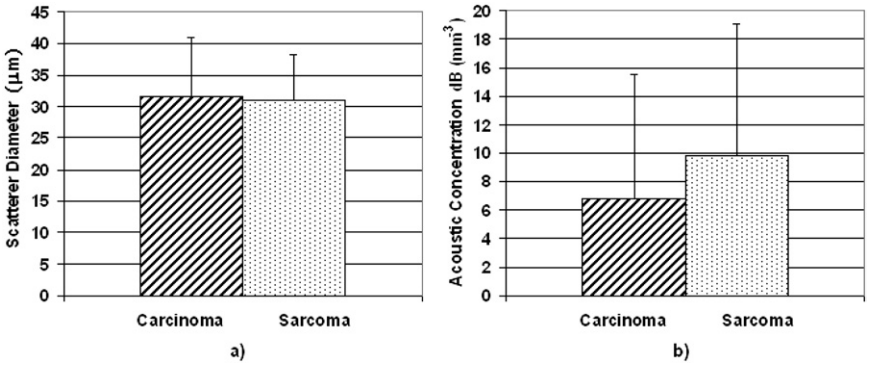

Fig. 2. Histograms representing the (a) ASD and (b) the AAC estimated from the 10 mouse carcinomas and 10 mouse sarcomas. The error bars represent one standard deviation.

benign mammary fibroadenomas in rodent models (Oelze et al. 2004). Examination of these images does not allow the distinguishing of the carcinomas from the sarcomas. The actual AAC values for both tumors are given in the histogram of Fig. 2b. The estimated AAC values for both tumors were 6.77 ± 8.75 dB (mm^{-3}) and 9.87 ± 9.24 dB (mm^{-3}) for the carcinomas and sarcomas, respectively. A statistically significant difference was not observed between the carcinomas and sarcomas from the AAC estimates ($p = 0.86$).

A feature analysis plot (Fig. 4) of the AAC *vs.* the ASD indicates that the carcinomas and sarcomas are not separable based on the scatterer property estimates obtained by using the spherical Gaussian model for ultrasound backscatter with the initial analysis bandwidth.

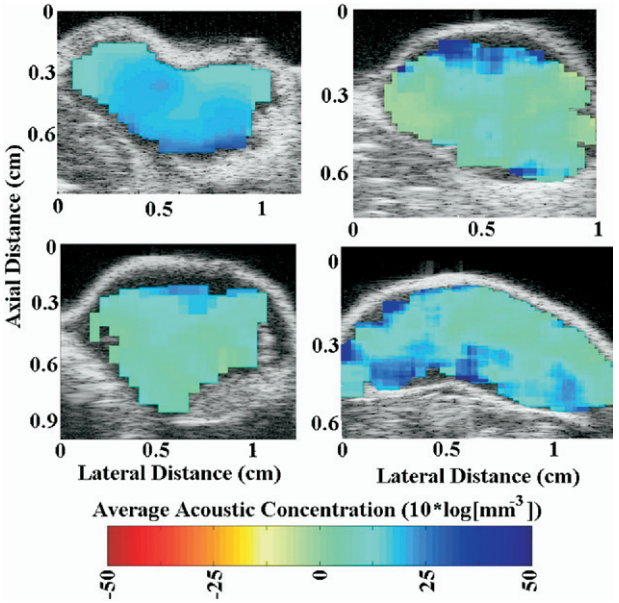

Fig. 3. AAC images of mouse carcinomas (left panel) and mouse sarcomas (right panel).

The points representing the two different kinds of tumors fall on top of each other and no line can be drawn in Fig. 4 separating one kind of tumor from the other. Furthermore, examination of Fig. 4 reveals that larger ASD estimates correlate to smaller AAC estimates.

Examination of optical photomicrographs of the two kinds of tumors did reveal significant structural differences between the carcinomas and sarcomas. Figure 5a and b are optical photomicrographs of the carcinomas and sarcomas. The carcinomas had relatively uniform morphology (*i.e.*, homogenous scatterer environment) and minimal extracellular matrix. The cells were oval to polygonal in shape with prominent nuclei and a cytoplasmic volume 50% to 200% greater than the nuclear volume. The ratio of cytoplasmic area relative to nuclear area was made by visually estimating the nuclear area from the two-dimensional (2-D) optical photomicrographs of the tumors and the total area of the photomicrograph slide. The average nuclear diameter was calculated to be 13 μm, and details of this analysis can be found in Oelze et al. (2004). If the average nuclear

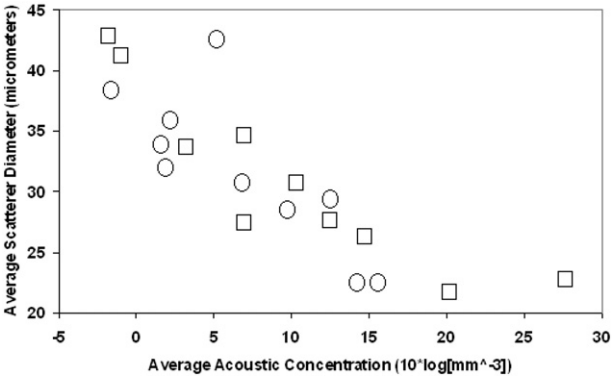

Fig. 4. Feature analysis plot of the AAC *vs.* the ASD for the 10 mouse carcinomas, ○, and 10 mouse sarcomas, □, using the analysis bandwidth of 10 to 25 MHz.

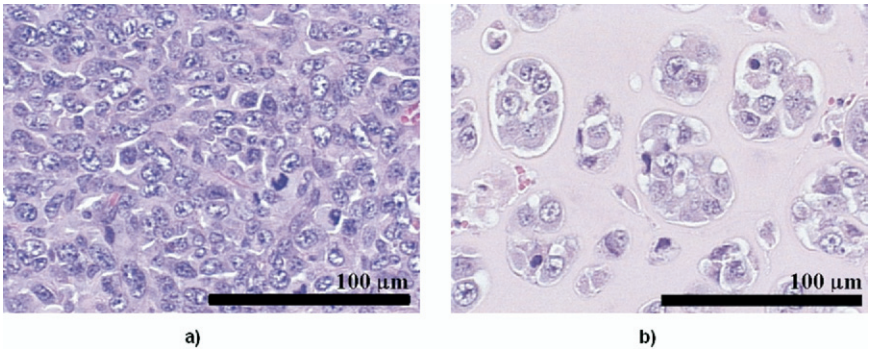

Fig. 5. Optical photomicrographs of (a) a mouse carcinoma and (b) a mouse sarcoma.

diameter was 13 μm and total cell volume was 50% to 200% larger than the nuclear volume, then the total cell diameter ranged between 20 and 39 μm. Comparison of the cell sizes estimated from the optical photomicrographs and ultrasound ASD estimates suggested the cells could be a significant source of backscatter.

To test the importance of cells to scattering, carcinoma cells grown in culture were examined using the ultrasound system and QUS technique. The carcinoma cells were grown in culture, harvested, and gently centrifuged at 900 rpm for 10 min into a pellet. The pellet was placed in a tube of 1-cm diameter and covered with Saran® wrap to act as a scanning window. Figure 6 is an ASD image of the cell pellet. The ASD estimated from the carcinoma cell pellet was 28.0 $\pm$ 9.00 μm. No statistically significant differences existed between the ASD estimates of the cell pellets and carcinoma tumors. No comparisons were made between the sarcoma tumors and cell pellets of the sarcoma cells because the sarcoma cells were cultured *in vivo* and therefore not amenable to pelleting.

The sarcomas (Fig. 5b) were similar to the carcinomas (Fig. 5a) in that the average nuclear size appeared to be approximately the same for both. However, instead of a uniform distribution of cells within the tumor, the cells in the sarcomas were arranged in groups that ranged from one cell diameter in size to almost 100 μm in diameter. The clumped structures were surrounded by an extracellular matrix consisting of collagen IV, entactin, and heparan sulfate proteoglycan (essentially a gel-like material [matrigel]) (Kleinman et al. 1986; Timpl et al. 1979).

While the technique is system-independent and correlation appeared to exist between ASD estimates and average cell sizes, the technique was unable to distinguish between the two kinds of tumors interrogated. The biologic variance between the carcinoma and sarcoma microstructure observed in the optical photomicrographs

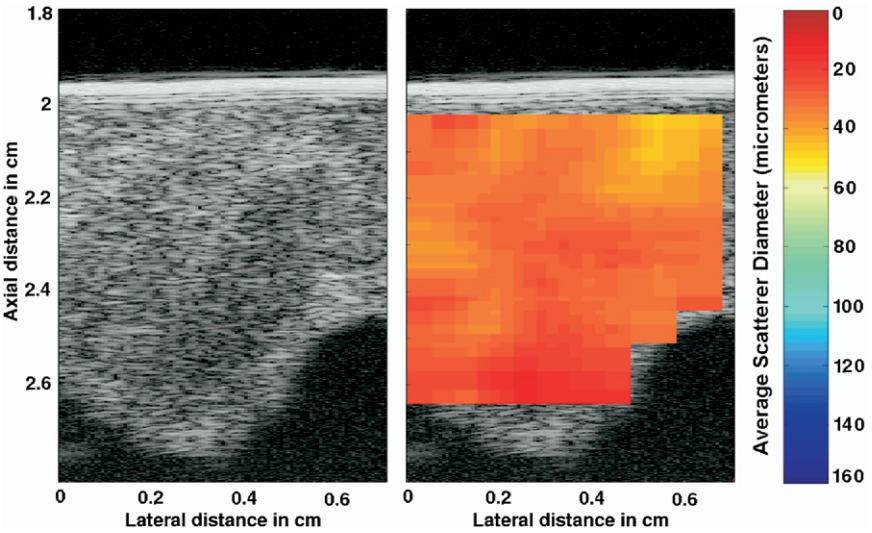

Fig. 6. Grey-scale B-mode image of a carcinoma cell pellet and ASD image of the carcinoma cell pellet.

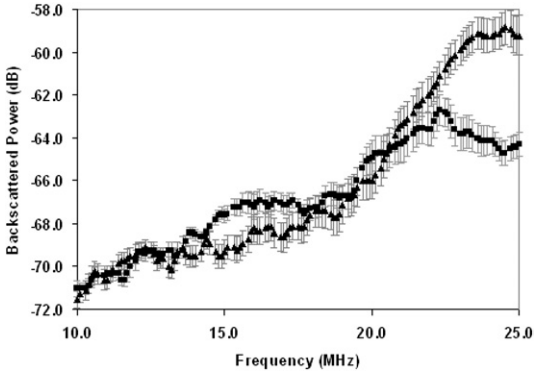

Fig. 7. Images of the averaged power spectra from the carcinomas, ■, and sarcomas, ▲ Error bars represent the standard error of the average spectra for the 10 animals.

did not translate into statistically significant differences between the estimates of the scatterer properties of the carcinomas and sarcomas using the current QUS analysis. One hypothesis explaining the failure of the current QUS analysis to distinguish between the carcinoma and sarcoma is that the model being used for scattering estimates was not sensitive to these differences observed microscopically. Because the spherical Gaussian model is a predictor of the backscattered power spectrum, to test the hypothesis, F-tests using two-way ANOVA were conducted on the averaged power spectra from the carcinomas and sarcomas.

The F-test can be used to determine if one curve does not fit another curve by comparing the variance between each sampled point between the curves. An F-test on two curves indicates whether there exist statistically significant differences between the two curves being compared. Figure 7 is a graph of the averaged power spectra from the carcinomas and sarcomas. F-tests conducted on the averaged power spectra from the carcinomas and sarcomas did not indicate statistically significant differences ($p = 1.0$) over the analysis bandwidth (10 to 25 MHz). However, posttests on different frequency bands indicated that the largest bandwidth over which statistically significant differences between the two curves existed was over the frequency range of 16 to 25 MHz ($p < 0.05$). The F-tests indicated that statistically significant differences existed between the backscattered power spectra from the carcinomas and sarcomas over the frequency ranges 16 to 25 MHz that were not revealed by the spherical Gaussian model over the initial analysis bandwidth (10 to 25 MHz).

Based on the results of the F-tests, ASD and AAC estimates were obtained by means of the spherical Gaussian model using a new analysis bandwidth of 16 to 25 MHz. The estimated ASD values were 42.0 ± 4.01 μm and 32.1 ± 3.81 μm for the carcinomas and sarcomas, respectively. The estimated AAC values were 16.4 ± 17.1 dB (mm^{-3}) and 36.4 ± 11.9 dB (mm^{-3}) for the carcinomas and sarcomas, respectively. Statistically significant differences were observed using both the ASD and AAC estimates between the carcinomas and sarcomas with the new analysis bandwidth. The feature analysis plot (Fig. 8) using the new analysis bandwidth reveals a separation between the carcinoma and sarcoma estimates.

DISCUSSION

Two animal models for cancer were examined using QUS and optical microscopy. The QUS analysis was based on the spherical Gaussian model to parameterize the backscattered power spectra from tumors and estimate scatterer properties. The goals of this QUS analysis were to: (1) develop a system-independent technique for quantifying tissue, (2) relate the scatterer property estimates to underlying tissue microstructure, and (3) distinguish between different kinds of tumors based on the quantified information (scatterer properties). Because of the procedures for normalizing the backscattered power spectra, the QUS technique can be considered system-independent.

Examination of the optical photomicrographs of the tumors suggested that the cells were the structures inside the tumors most likely responsible for the measured backscatter. In the case of the carcinomas, the cells were uniform in size and shape and distributed as solid sheets of cells throughout the tumor. In the case of the sarcomas, the cells were uniform in size and shape but arranged in groups of cells distributed at random in the extracellular matrix throughout the tumor. The differences in the way the cells were distributed in the two tumors suggest that the AAC should be an important parameter for revealing these differences. However, no

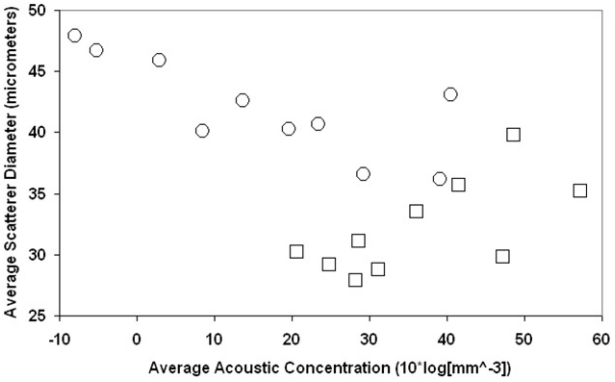

Fig. 8. Feature analysis plot of the AAC *vs.* the ASD for the 10 mouse carcinomas, ○, and 10 mouse sarcomas, □, using the analysis bandwidth of 16 to 25 MHz.

statistically significant differences were observed using QUS with the initial analysis bandwidth of 10 to 25 MHz and the spherical Gaussian model. We hypothesize that the failure to detect differences using the initial analysis bandwidth was due to the spherical Gaussian model not being sensitive to features of the backscattered power spectra that could identify these differences.

Further evidence supporting the hypothesis that cells were responsible for scattering came from examination of pellets of the carcinoma cells grown in culture. No statistically significant differences were observed between ASD estimates from the tumors and cell pellets. The similarity between ASD estimates suggests that cells were responsible for backscatter from the cell pellets and from the carcinoma tumor.

In the analysis of both tumors, a correlation between the ASD and the AAC existed. Examination of Fig. 4 revealed that larger ASD estimates correlated to smaller AAC estimates. Two possibilities may explain this correlation. First, if larger scatterers exist in a tissue, then fewer of these scatterers can be contained within a unit volume. Therefore, larger scatterers lead to smaller estimates of AAC (number density is smaller). Second, if the ASD is overestimated, then estimates of AAC will be underestimated because the AAC is estimated from the slope parameter of eqn (4), which is a function of the ASD.

The QUS analysis was not successful at distinguishing between the carcinomas and sarcomas using the spherical Gaussian model over the analysis bandwidth of 10 to 25 MHz. Scatterer property estimates were not significantly different between the carcinomas and sarcomas. The two kinds of tumors could be distinguished from the optical photomicrographs but could not be distinguished from the scatterer property estimates using the spherical Gaussian model over the 10 to 25 MHz analysis bandwidth.

Although QUS is capable of differentiating between benign and malignant cancers (Oelze et al. 2004), the variance of scatterer property estimates was not small enough to differentiate between different kinds of malignant cancer (the carcinomas and sarcomas) using the spherical Gaussian model over the initial analysis bandwidth (10 to 25 MHz). However, F-tests revealed that significant differences existed between the average backscattered power spectra of the carcinomas and sarcomas over the bandwidth 16 MHz to 25 MHz. The differences suggest that better scattering models are needed to discriminate between the carcinomas and sarcomas over a large bandwidth or that appropriate frequency ranges for analysis need to be used with current models.

New ASD and AAC estimates were obtained by using the spherical Gaussian model over the portion of the bandwidth of the averaged backscattered power spectra, 16 to 25 MHz, where F-tests revealed statistical differences existed between the sarcomas and carcinomas. Several important results occurred from using the analysis bandwidth of 16 to 25 MHz over the initial analysis bandwidth. First, statistically significant differences between the carcinomas and sarcomas were observed. The separation between the estimates from the carcinomas and sarcomas can be observed in the feature analysis plot of Fig. 8. Second, the standard deviation of ASD estimates was reduced by almost half using the 16 to 25 MHz analysis bandwidth. If ASD estimates are more precise, then ASD estimates will be a better parameter for classifying tissues. Third, the analysis revealed that the spherical Gaussian model was adequate to detect the differences from the two kinds of tumors given that the appropriate frequency ranges were used. The results suggest that care should be taken in choosing an appropriate analysis bandwidth when using a model like the spherical Gaussian model.

Comparing QUS estimates with the underlying morphology did not reveal a one-to-one relationship of ASDs with actual structures. If the hypothesis that cells were the dominant source of scatter was correct, than ASD estimates should have been nearly identical between the carcinomas and sarcomas. Second, because of the abundant extracellular matrix in the sarcomas (lower cell number density), the AAC estimates for sarcomas should have been less than the AAC estimates for the carcinomas. The results using the 16 to 25 MHz analysis bandwidth revealed statistically significant differences in ASD estimates and yielded AAC estimates for the sarcomas that were much larger than AAC estimates for the carcinomas. Therefore, either the hypothesis that cells are the dominant source of scattering is wrong or other effects not accounted for in the theory exist. The ASD estimates from the cell pellets support the hypothesis that cells are a dominant source of backscatter in the tumors; therefore, other possible effects not taken into account by the theory should be examined. Some researchers have suggested that in tumors with a tightly packed, uniform distribution of cells, the assumption of a random scattering medium may be violated (Hunt et al. 2002; Tunis et al. 2005). Periodic structures in the tumors, if not taken into account, will affect the ASD and AAC estimates. More study needs to be conducted to determine the effects on scatterer property estimates of periodicities in the scattering medium.

Because F-tests indicated statistical differences over the frequency ranges of 16 MHz to 25 MHz, the application of the QUS techniques in clinical situations may be limited to superficial cancer detection and classification. To observe microstructural changes at the level of the cells and cell growth patterns, high ultrasonic frequencies must be used ($>$16 MHz in the two cases

examined). For example, the most precise scatterer size estimates can be made when $ka \sim 1.0$ (Insana et al. 1990). At 20 MHz in tissue (speed of sound ~1540 m/s), QUS is most sensitive to ASD estimates of 24.5 μm (about the size of the cancer cells examined). Due to tissue attenuation, examination of deep-seeded tumors with high-frequency ultrasound (>16 MHz) may not be possible. However, for superficial cancers (*e.g.*, ocular, thyroid, cervical, prostate, skin and superficial breast tumors) interrogating with higher frequency ultrasound and QUS techniques is possible.

Acknowledgements—We acknowledge the technical assistance of Rita J. Miller and James P. Blue, Jr., on this project. The authors recognize that the pioneering work of the late Dr. Frederic Lizzi has led to the present study. This work was supported by NIH F32 CA96419 (to MLO) and by start-up funds provided by the Department of Electrical and Computer Engineering at the University of Illinois at Urbana-Champaign.

REFERENCES

Aslakson CJ, Miller FR. Selective events in the metastatic process defined by analysis of the sequential dissemination of subpopulations of a mouse mammary tumor. Cancer Res 1992;52:1399–1405.

Balaji KC, Fair WR, Feleppa EJ, et al. Role of advanced 2 and 3-dimensional ultrasound for detecting prostate cancer. J Urol 2002;168:2422–2425.

Cotran RS, V Kumar, T Collins Pathologic basis of disease (6th ed) Philadelphia: WB. Saunders Co., 1999.

Drukker K, Giger ML, Horsch K, et al. Computerized lesion detection on breast ultrasound. Med Phys 2002;29:1438–1446.

Feleppa EJ, Lizzi FL, Coleman DJ, Yaremko MM. Diagnostic spectrum analysis in ophthalmology: A physical perspective. Ultrasound Med Biol 1986;12:623–631.

Feleppa EJ, Lizzi FL, Coleman DJ. Ultrasonic analysis for ocular tumor characterization and therapy assessment. News Physiol Sci 1988; 3:193–197.

Feleppa EJ, Kalisz A, Sokil-Melgar JB, et al. Typing of prostate tissue by ultrasonic spectrum analysis. IEEE Trans Ultrason Ferro Freq Cont 1996;43:609–619.

Feleppa EJ, Liu T, Kalisz A, et al. Ultrasonic spectral-parameter imaging of the prostate. Int J Imaging Syst Technol 1997;8:11–25.

Feleppa EJ, Fair WR, Tsai H, et al. Progress in two-dimensional and three-dimensional ultrasonic tissue-type imaging of the prostate based on spectrum analysis and nonlinear classifiers. Molec Urol 1999;3:303–310.

Garra BS, Insana MF, Sesterhenn IA, et al. Quantitative ultrasonic detection of parenchymal structural change in diffuse renal disease. Invest Rad 1994;29:134–140.

Hall TJ, Insana MF, Harrison LA, Cox GG. Ultrasonic measurement of glomerular diameters in normal adult humans Ultrasound Med Biol 1996;22:987–997.

Hunt JW, Worthington AE, Xuan A, et al. A model based upon pseudo regular spacing of cells combined with the randomization of the nuclei can explain the significant changes in high-frequency ultrasound signals during apoptosis. Ultrasound Med Biol 2002;28:217–226.

Insana MF, Wagner RF, Brown DG, Hall TJ Describing small-scale structure in random media using pulse-echo ultrasound. J Acoust Soc Am 1990;87:179–192.

Insana MF, Hall TJ. Parametric ultrasound imaging from backscatter coefficient measurements—Image-formation and interpretation. Ultrasonic Imag 1990;12:245–267.

Insana MF, Hall TJ, Fishback JL. Identifying acoustic scattering sources in normal renal parenchyma from the anisotropy in acoustic properties. Ultrasound Med Biol 1991;17:613–626.

Insana MF, Wood JG, Hall TJ. Identifying acoustic scattering sources in normal renal parenchyma in vivo by varying arterial and ureteral pressures. Ultrasound Med Biol 1992;18:587–599.

Insana MF, Brown DG. Acoustic scattering theory applied to soft biological tissues. In: Shung KK, Thieme GA, eds. Ultrasonic scattering in biological tissues. Boca Raton, FL: CRC Press, 1993:75–124.

Ishimaru A. Wave propagation and scattering in random media. New York: Academic Press, 1978:331–334.

Kleinman HK, McGarvey ML, Hassell JR, et al. Basement membrane complexes with biological activity. Biochemistry 1986;25:312–318.

Lizzi FL, Greenebaum M, Feleppa EJ, Elbaum M, Coleman DJ. Theoretical framework for spectrum analysis in ultrasonic tissue characterization. J Acoust Soc Am 1983;73:1366–1373.

Lizzi FL, Ostromogilsky M, Feleppa EJ, Rorke MC, Yaremko MM. Relationship Of ultrasonic spectral parameters to features of tissue microstructure. IEEE Trans Ultrason Ferro Freq Cont 1987;34: 319–329.

Lizzi FL, Astor M, Liu T, et al. Ultrasonic spectrum analysis for tissue assays and therapy evaluation. Int J Imaging Syst Technol 1997a; 8:3–10.

Lizzi FL, Feleppa EJ, Astor M, Kalisz. Statistics of ultrasonic spectral parameters for prostate and liver examinations. IEEE Trans Ultrason Ferro Freq Cont 1997b;44:935–942.

Miller JG, Perez JE, Mottley JG, et al. Myocardial tissue characterization: An approach based on quantitative backscatter and attenuation. Ultrasonics Symp Proc 1983;2:782–793.

Morse PM, Ingard KU. Theoretical acoustics. New York: McGraw-Hill, 1968.

Nassiri DK, Hill CR. The use of angular scattering measurements to estimate structural parameters of human and animal tissues. J Acoust Soc Am 1986;79:2048–2054.

Nicholas D. Evaluation of backscattering coefficients for excised human tissues: Results interpretation, and associated measurements. Ultrasound Med Biol 1982;8:17–28.

Oelze ML, O'Brien WD Jr. Frequency-dependent attenuation-compensation functions for ultrasonic signals backscattered from random media. J Acous Soc Am 2002;111:2308–2319.

Oelze ML, Zachary JF, O'Brien WD Jr. Characterization of tissue microstructure using ultrasonic backscatter: Theory and technique optimization using a Gaussian form factor. J Acoust Soc Am 2002;112:1202–1211.

Oelze ML, Zachary JF, O'Brien WD Jr. Differentiation and characterization of mammary fibroadenomas and 4T1 Carcinomas using ultrasound parametric imaging. IEEE Trans Med Imag 2004;23:764–771.

Pulaski BA, Ostrand-Rosenberg S. Reduction of established spontaneous mammary carcinoma metastases following immunotherapy with major histocompatibility complex class II and B7.1 cell-based tumor vaccines. Cancer Res 1998;58:1486–1493.

Pulaski BA, Terman DS, Kahn S, Muller E, Ostrand-Rosenberg S. Cooperativity of *Staphylococcal aureus* enterotoxin B superantigen, major histocompatibility complex class H, and CD80 for immunotherapy of advanced spontaneous metastases in a clinically relevant postoperative mouse breast cancer model. Cancer Res 2000;60:2710–2715.

Silverman RH, Rondeau MJ, Lizzi FL, Coleman DJ. Three-dimensional high-frequency ultrasonic parameter imaging of anterior segment pathology. Ophthalmology 1995;102:837–843.

Silverman RH, Folberg R, Boldt HC, et al. Correlation of ultrasound parameter imaging with microcirculatory patterns in uveal melanomas. Ultrasound Med Biol 1997;23:573–581.

Stavros AT, Thickman D, Rapp CL, et al. Solid breast nodules: Use of sonography to distinguish between benign and malignant lesions. Radiology 1995;196:123–134.

Timpl R, Rohde H, Robey PG, et al. Laminin—A glycoprotein from basement membranes. J Biol Chem 1979;254:9933–9937.

Tunis AS, Czarnota GJ, Giles A, et al. Monitoring structural changes in cells with high-frequency ultrasound signal statistics. Ultrasound Med Biol 2005;31:1041–1049.